Size-scaling of Electronic and Magnetic Properties of Triangular Graphene Nanoflakes

WANG Yizhe[1,2], ZHAO Guodong[1,2], LIU Chao[1,2], LI Yongchang[1,2], LIU Chang[1,2], WANG Yin[2,3], KONG Xiangyang[4], ZHANG Peihong[5], REN Wei[1,2†]

1. *Materials Genome Institute, State Key Laboratory of Advanced Special Steel, Physics Department, Shanghai University, Shanghai* 200444;
2. *International Centre for Quantum and Molecular Structures, Shanghai Key Laboratory of High Temperature Superconductors, Shanghai University, Shanghai* 200444;
3. *Hongzhiwei Technology (Shanghai) Co. Ltd., Shanghai* 201206;
4. *Institute of Materials for Mobile Energy, School of Materials Science and Engineering, Shanghai Jiao Tong University, Shanghai*, 200240;
5. *Department of Physics, University at Buffalo, State University of New York, Buffalo, New York* 14260

Received date: 2021-06-01; accepted date: 2021-06-15

【Abstract】 We employ density functional theory (DFT) to investigate the electronic and magnetic properties of hydrogen passivated equilateral triangular graphene nanoflake (GNF). It is predicted that the ground state of such graphene nanostructure exhibits robust magnetic edge states and strong quantum confinement effects. Our DFT calculations based on different exchange-correlation functionals demonstrate that the electronic energy gap and local magnetic moment of GNFs depend sensitively on the GNF size. This is attributed to the different numbers of atoms in the two sublattices of graphene since the spins on the same and different sublattices couple ferromagnetically and antiferromagnetically, respectively. The total net magnetic moment scales linearly with the size of nanoflakes, while the average magnetic moment localized at edges increases and saturates to a constant value for larger sizes. We show that the spin-flipped and spin-preserving energy gaps near Fermi level decrease as the size of GNFs increases. The degeneracies near Fermi energy are proportional to the length of edge in these triangular zigzag-edged GNFs as well. The electronic and magnetic properties of GNFs thus open new avenues for utilizing triangular graphene in nanoscale magnetic semiconductor and optoelectronic devices.

Keywords: graphene nanoflakes, quantum confinement, edge states, density functional theory

PACS: 32. 10. Dk, 73. 21. La, 73. 22. Pr, 75. 75. -c

DOI: 10.13380/j.ltpl.2021.02.006

Reference method: WANG Yizhe, ZHAO Guodong, LIU Chao, LI Yongchang, LIU Chang, WANG Yin, KONG Xiangyang, ZHANG Peihong, REN Wei, Low. Temp. Phys. Lett. **43**, 0115 (2021)

三角形石墨烯纳米片电子和磁学性质的尺寸效应

王裔喆[1,2],赵国栋[1,2],刘超[1,2],李永昌[1,2],刘畅[1,2],

* This work was supported by the National Natural Science Foundation of China (51861145315, 11929401, 12074241), the Independent Research and Development Project of State Key Laboratory of Advanced Special Steel, Shanghai Key Laboratory of Advanced Ferrometallurgy, Shanghai University (SKLASS 2020-Z07), the Science and Technology Commission of Shanghai Municipality (19DZ2270200, 19010500500, 20501130600), and High Performance Computing Center, Shanghai University. † renwei@shu.edu.cn

王音[3],孔向阳[4],张培鸿[5],任伟[1,2†]

1. 上海大学材料基因组工程研究院,省部共建高品质特殊钢冶金与制备国家重点实验室,物理系,上海 200444;

2. 上海大学量子与分子结构国际研究中心,上海市高温超导重点实验室,上海 200444;

3. 鸿之微科技(上海)股份有限公司,上海 201206;

4. 上海交通大学材料科学与工程学院,汽车动力电池材料研究所,上海 200240;

5. 纽约州立大学布法罗分校物理系,纽约 14260

收稿日期:2021-06-01;接收日期:2021-06-15

【摘要】 基于密度泛函理论,本文研究了氢钝化锯齿形边缘三角形石墨烯纳米片的电子结构和磁学性质,这种石墨烯纳米结构的基态表现出强烈的磁性边缘态和量子尺寸效应。我们应用多种交换关联泛函,对体系的自旋密度和电子结构进行了第一性原理计算和理论分析,结果表明三角形石墨烯纳米片的总磁矩和自旋随尺寸线性变化,平均磁矩随着尺寸变大而增加,并逐渐趋于一个定值。与此同时,体系的能隙随着尺寸增加而减小,其中自旋不变能隙的调控对光学响应和光子激发有着重要意义。计算得到的单电子能谱表明,费米能级的简并度与体系尺寸成正比。应用多种交换关联泛函的计算结果表明,三角形石墨烯纳米片具有可调控的自旋和能隙,为其在纳米级光电器件和磁性半导体的应用方面提供了理论依据.

关键词:石墨烯纳米片,量子尺寸效应,边界态,密度泛函理论

PACS: 32. 10. Dk, 73. 21. La, 73. 22. Pr, 75. 75. -c

DOI: 10.13380/j.ltpl.2021.02.006

1 Introduction

It is well known that magnetism in solids is usually attributed to either *d* or *f* electrons, and therefore carbon-based materials are generally regarded as non-magnetic. Nevertheless, it was showed that intrinsic magnetism might exist in *s*-*p* electron systems, and such magnetic order was predicted to be stable even at room temperature[1,2]. Since graphene was successfully exfoliated in experiment[3], the low-dimensional carbon-based materials have drawn enormous attention due to their extraordinary properties including electronic conductivity[4], superconductivity[5−6], and high carrier mobility[7]. Graphene is a kind of one-atom-thick carbon layer of graphite, made up of a honeycomb lattice in two dimensions. Although the ideal graphene's nonmagnetic ground state holds back its application in spintronics[8], recent studies have found the emergence of long-range magnetic order on the zigzag edges in the graphene-derived structures when going to lower dimensions (e. g. quasi-one-dimensional nanoribbon[9-13] and zero-dimensional nanoflakes[14-18]. Graphene nanoflakes (GNFs), or nanodisks, nanoislands and quantum dots, have different shapes and sizes, which might be realized by synthesizing from smaller molecules or cutting from a graphene sheet. Recently, the fabrication and characterization of various graphene-based nanodevices[19-21] provided access to detailed knowledge of graphene-derived structures. In this context, GNFs have been identified as attractive candidates for spin qubits and quantum information storage[22-24]. The synthesis of triangular GNFs, however, is extremely challenging due to the enhanced chemical instability[25]. Their open-shell structures and the presence of unpaired electrons make such *triangulene* difficult to fabricate. Nevertheless, triangular GNFs have been synthesized by using the bottom-up on-surface approach[26-28], with atomic precision. Although the magnetic properties of exactly triangular-shaped GNFs have not been well understood experimentally[29], the nanoflakes with a triangular shape were predicted[26] to host nonzero magnetic moments mainly on their zigzag edges, and the local magnetization decays inwards and tends to disappear in the middle of the graphene fragment.

The nonzero net spin of triangular GNFs is attributed to its distinctive honeycomb framework containing $(n-1)$ unpaired electrons[16,27-28,30-31]. The lattice of graphene is formed by two sublattices, namely A and B. In *triangulene*, the numbers of atoms in the two sublattices are not equal, $N_A \neq N_B$. The total spin value S scales linearly with $(N_A - N_B)$ (and the GNF size as well), which could be anticipated from Lieb's theorem[32]. Using the Hubbard model with a bipartite lattice and a half-filled band, it was shown that the ground state has $S = (N_A - N_B)/2$. In triangular shaped quantum dots, the sublattice imbalance $N_A - N_B = n-1$, where n number of sublattice A atoms on one edge of the triangulene. Thus, the net spin always satisfies $S = (n-1)/2$. It would be interesting and important to investigate the finite-size effects on the electronic and magnetic properties of nanoflakes. In this work, we characterize the flake size of GNFs by the index n. We carried out first-principles calculations to explore the magnetic and energetic properties of triangular zigzag-edged n-GNFs with the edge lengths in the range of 0. 68 to 5. 11 nm (from 2-GNF to 20-GNF). The largest flake contains 481 carbon atoms as shown in Fig. 1(a). We investigate the magnetic moment and energy gap as functions of size; the degeneracy at Fermi level is also analyzed for the spin-polarized ground states. This investigation provides quantitative understanding of the size-scaling behavior of the magnetic and electronic properties of triangular graphene nanoflakes with hydrogenated zigzag edges.

2 Methods

Our calculations were carried out based on

spin polarized density functional theory (DFT), using projector-augmented wave (PAW) method[33,34] as implemented in Vienna *ab initio* simulation package (VASP)[35-36]. One Gamma *k*-point sampling was used, and the electronic wavefunctions were expanded using a plane-wave basis set with a cutoff energy of 500 eV, which gave rise to good convergence for the energy (10^{-5} eV). The structures of all GNFs are optimized until the force on each atom is smaller than 0.01 eV/Å. The spin-polarized local density approximation (LDA)[37], Perdew-Burke-Ernzerhof (PBE)[38] of generalized gradient approximation (GGA)[39-40], and PBEsol[41] exchange-correlation functionals were employed for the DFT computations. The calculated spin density isosurfaces were plotted using VESTA[42].

3 Results and discussion

We have constructed and optimized structures of a set of triangular GNFs with different triangle edge sizes, in which each carbon atom at edges is bonded to a single hydrogen atom. The monohydrogenated flakes were found to retain triangular shape after optimization regardless of their sizes and exchange-correlation functionals. Besides, each carbon ring in nanoflakes keeps its hexagonal shape from the edge to central regions. As shown in Fig. 1, the edges of the triangular GNFs are passivated by hydrogen atoms to eliminate dangling bonds. We summarized the calculated edge lengths and bond lengths of a series of optimized triangular hydrogenated GNFs with $n = 2, 3, \cdots, 9, 10$. Using the PBE functional, it was found that bond lengths change significantly compared with ideal graphene. The length of the C-C bonds located at the three corners of *n*-GNFs is 1.39 Å, which is slightly shorter than other C-C bonds (1.41 ~ 1.44 Å) at the edge and the inner area; the length of H-C bonds is 1.09 Å. For larger GNFs with $n = 11, 12, \cdots, 19, 20$, we adopted the structure of pristine graphene, with the H-C bonds fixed at 1.09 Å and C-C bonds 1.42 Å. In Fig. 1(a), we show the 20-GNF *triangulene* consisting of $n^2 + 4n + 1 = 481$ C atoms and $3n + 3 = 63$ H atoms. The length of the edge is about 51 Å. The honeycomb lattice of GNFs formed by two sublattices A and B is shown in Fig. 1(b), with $N_A - N_B = n - 1 = 19$ for 20-GNF.

We employed three different energy functions to investigate the magnetism and electronic structures of GNFs of different sizes. Our results show that the total magnetic moment increases with the nanoflake size, regardless of the functional used. Meanwhile, the energy gaps are found to decrease monotonically (except for the phenalenyl 2-GNF) with increasing nanoflake size. Note that at large*n* limit, we expect a disappearance of band gap for the infinite sized graphene. Our calculations suggest that the ground states of triangular nanoflakes with zigzag edges are intrinsically magnetic, with spin ferromagnetically coupled within the sublattice and antiferromagnetically coupled between the two sublattices, giving rise to a ferrimagnetic ordering in the triangular nanoflakes. The ferrimagnetic ordering is clearly seen by plotting the spin density isosurfaces as shown in Fig. 1(c)~(h). The spin polarization density is defined as $M(r) = \rho_{\uparrow}(r) - \rho_{\downarrow}(r)$. The net spin $S = (N_{\uparrow} - N_{\downarrow})/2$ where $N_{\uparrow}$ and $N_{\downarrow}$ correspond to the number of atoms localized up and down magnetic moments, respectively, and thus satisfies $S = (N_A - N_B)/2 = (n-1)/2$.

The spin densities for 10-GNF at LDA, PBEsol, and PBE levels are shown in Fig. 1(c)~(e), respectively, where different colors indicate different spin states: blue is for the up-spin moment while red for down-spin moment. In the zigzag edged triangle-shaped GNF structure, the up-spin moment prefers to localize on sublattice A while down-spin moment prefers to localize on B, giving rise to a net spin-up magnetic state. This is to minimize the on-site Coulomb repulsion and prevent a double occupation of one p_z orbital at the

same carbon site[32,43].

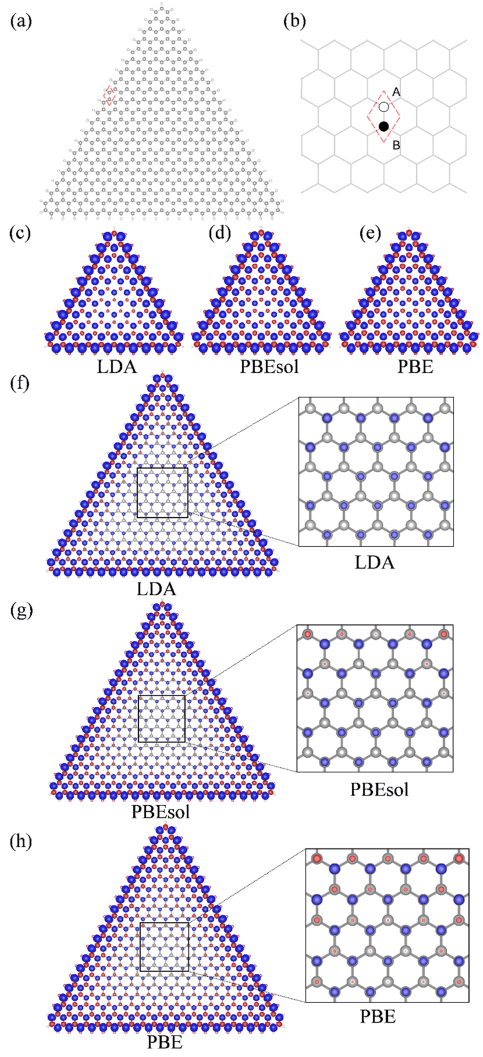

Fig. 1 Atomic structure and spin density of triangle shaped GNFs. (a) One H atom (small and white) is attached to each of the outmost C atoms (big and grey) at three edges in 20-GNF. (b) Two-dimensional crystalline lattice of graphene. The area indicated by red dashed line represents the unit cell of graphene containing two carbon atoms which belong to the two sublattices of graphene, namely A (empty circle) and B (filled circle). Spin density of 10-GNF obtained through DFT calculation using (c) LDA, (d) PBEsol, and (e) PBE functionals. (f)-(h) The spin density of 20-GNF is calculated by using those three functionals. Blue / red isosurfaces correspond to the spin up / down density. The magnitudes of up and down spin moments are proportional to the size of the spheres. The isosurfaces of spin density are drawn using VESTA[42].

In Fig. 1, we present the spin density of 10-GNF in (c)-(e) and that of 20-GNF in (f)-(h). It is illustrated clearly that magnetic moments of triangular nanoflakes develop mainly along the edges. In addition, we find that the larger the size of GNFs, the more localized the edge states. For the largest nanoflake, 20-GNF, the total magnetic moment is $M=19\ \mu_B$. It is interesting that such a large magnetic moment can develop in a nanoscale s-p system. We compared the isosurfaces of spin density calculated using three DFT functionals and found only small differences, suggesting the robustness of the magnetism in these nanoflakes. Inspecting the spin density for 20-GNF calculated within the LDA in Fig. 1(f), we observe that the local magnetic moments sit mainly on the edges, then decay rapidly and vanish eventually when approaching to the center of the flake. For 20-GNF, as the magnetic moments are mainly localized on three edges, atoms near the center of the nanoflake have negligible local moments ($\sim 0.004\ \mu_B$).

It is well know that the magnetic properties of graphene nanoribbon can be tuned by different hydrogen passivated schemes, we compare three other nanoflakes of different hydrogen passivation with the above discussed monohydrogenated GNFs ($C_{n^2+4n+1}H_{3n+3}$). We take 5-GNF as a representative example, considering bare nanoflake with no hydrogen passivated edges (C_{n^2+4n+1}), and nanoflakes with dihydrogenated carbon edges ($C_{n^2+4n+1}H_{6n+6}$) as well. Besides, we construct a special kind of corner-dihydrogenated nanoflake with three carbon atoms at corners saturated by two H atoms and other edge atoms bonded to one H atom ($C_{n^2+4n+1}H_{3n+6}$). Optimized structures for these four different hydrogen-passivated configurations are shown in Fig. 2.

Compared with our previous monohydrogenated configuration, the carbon atoms at edges or corners transform from sp^2 to sp and sp^3 types in bare, corner-dihydrogenated and dihydrogenated nanoflakes. This results in the different number of unpaired electrons in triangular

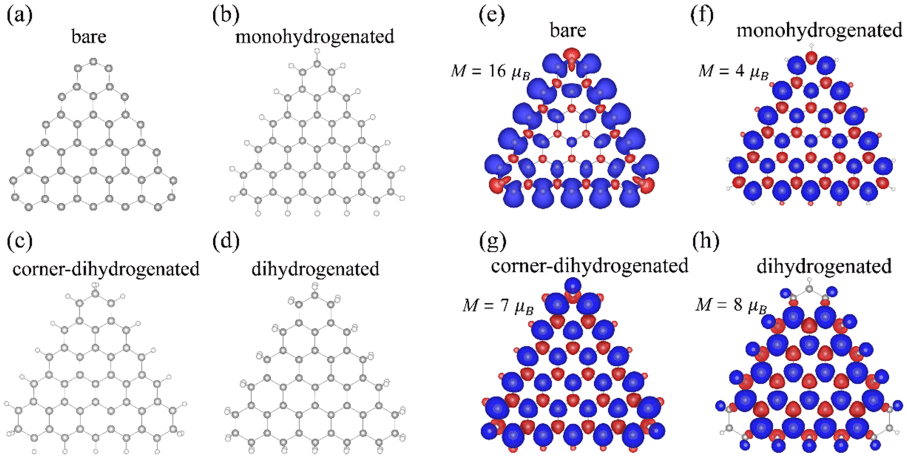

Fig. 2 Atomic structures of 5-GNFs with different hydrogen passivated schemes: (a) bare, (b) monohydrogenated, (c) corner-dihydrogenated and (d) dihydrogenated nanoflakes. Calculated spin density and total moments of nanoflakes are given in (e)-(h) for (a)-(d) respectively.

GNFs and therefore changes the total moments. We present the calculated spin density isosurface and total spin moments M for bare, monohydrogenated, corner-dihydrogenated and dihydrogenated nanoflakes in Fig. 2 (e)-(f). The calculated magnetic moment of the monohydrogenated case is 4 μ_B with 4 unpaired electrons. For bare 5-GNF, when all hydrogen atoms are removed the nanoflakes, each of $3n$ sublattice A atoms and three sublattice B atoms has an extra nonbonding electron that contributes to the magnetic moment, thus giving rise to a net magnetic moment $(n-1+3n-3)\ \mu_B = 16\ \mu_B$. For corner-dihydrogenated 5-GNF, three more hydrogen atoms than the monohydrogenated 5-GNF are passivated on the corner atoms. This induces three extra unpaired electrons and results in a total magnetic moment $(n-1+3)\ \mu_B = 7\ \mu_B$. For configuration shown in Fig. 2 (d), at three dihydrogenated edges, each carbon atom has sp^3 hybridized electrons, giving rise to a total magnetic moment $|n-1-3n+3|\ \mu_B = 8\ \mu_B$ and the spin-polarized orientation is reversed[44]. From these results, it will be interesting to obtain tunable magnetic moments of GNFs through various hydrogen saturation which might be applied in spintronic nanodevices.

Next, we continue to focus on the electronic and magnetic properties of triangular GNFs with monohydrogenated zigzag edges. We have also calculated the density of states and the energy spectra for a set of triangular zigzag-edged GNF with different sizes n as shown in Fig. 3. In Fig. 3(a) and Fig. 3(c), we present the projected density of states (PDOS) onto selected orbitals of carbon and hydrogen atoms of nanoflakes with $n = 10$ and 20 using the PBE functional. The vertical dashed lines denote the Fermi level, and the upper and lower panels show spin-up and spin-down states, respectively. Our calculations reveal that the highest occupied molecular orbital (HOMO) and lowest unoccupied molecular orbital (LUMO) are mainly contributed by the $2p_z$ orbitals of C atoms in GNFs. We note that the states near the Fermi level are strongly spin-polarized: the states below zero energy are the majority spin (up-spin) states, and those above are minority (down-spin) ones.

Fig. 3(b) and 3(d) show the energy levels calculated for 10-GNF and 20-GNF, respectively. Filled (empty) triangles represent occupied (unoccupied) energy levels, and blue and red colors distinguishes different spin orientations. The energy gaps are formed between up- and down-spin states, which are 0.49 eV for 10-GNF and 0.30 eV for 20-GNF, as shown in Figures. 3(b) and 3(d).

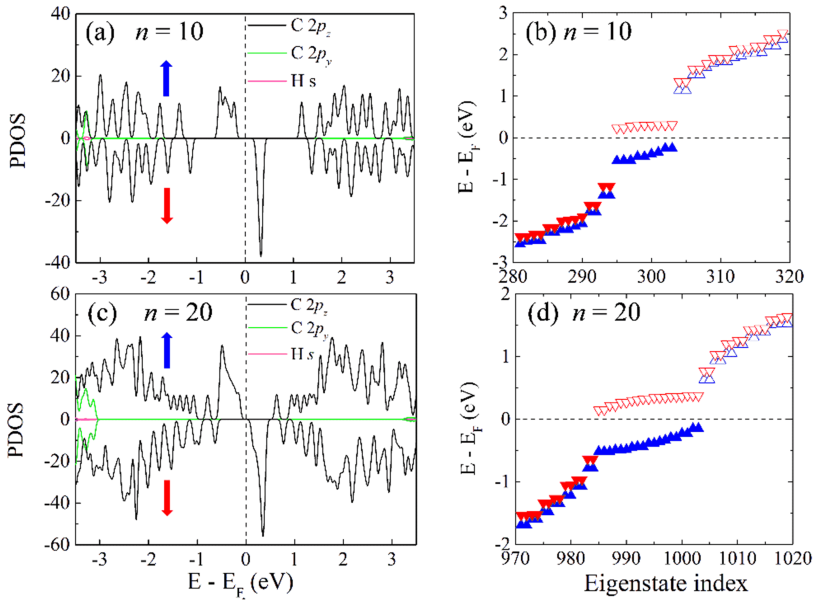

Fig. 3 Projected density of states (PDOS) and energy levels of GNFs calculated by using PBE functional. (a) and (b) show the PDOS and self-consistent energy levels respectively in triangular graphene nanoflake with $n = 10$. (c) and (d) show what in the nanoflake with $n = 20$. In (a) and (c), the vertical dashed line denotes the Fermi level, the upper and lower panels represent spin-up and spin-down states, respectively. In (b) and (d), the horizontal dashed line denotes the Fermi level, filled (empty) triangles represent occupied (un-occupied) energy levels, and, blue and red colors indicate spin up and down.

Here the energy gap is defined as the energy difference between the spin-up HOMO and spin-down LUMO, which are appropriate for processes involve spin flipping. We may also define spin-preserving gaps: up-spin gap is between the up-spin HOMO and LUMO, while down-spin gap is between the down-spin ones. The spin-preserving gaps are about 1.40 eV for 10-GNF and 0.78 eV for 20-GNF, with very little difference between the two spin channels. We mention that the spin-preserving gaps may be compared with optical excitations (if both electron-electron and electron-hole interactions are taken in account) in systems with weak spin-orbit coupling effects.

It is interesting to note that there is a very high degree of degeneracy for the states near the Fermi level (both in Figures. 3(b) and 3(d)), which coincides with the energy window in which significant spin-splitting are observed. In other words, spin polarization and splitting are accompanied with a high degree of degeneracy in a narrow energy range around the Fermi level ($E_F \pm 0.5$ eV). Therefore, the spin-polarization of the electronic states (so as the magnetic moment formation) comes exclusively at the band edges within a small energy window (± 0.5 eV) from the Fermi level. Outside this energy window, there is very small spin splitting between up- and down-spin states. This appears to be a unique feature of the magnetism in these nanoflakes. In addition, there are precisely $(n-1)$ spin-polarized states immediately below (majority spin) or above (minority spin) the Fermi level. Our results agree with previous works which show that the degeneracy at Fermi energy is equal to the difference between numbers of two sublattices in the bipartite lattice. Since there are $(n-1)$ more occupied up-spin states than down-spin states, the calculated net spin is 9/2 (19/2) for 10-GNF (20-GNF). It can be anticipated from the presence of $(n-1)$ unpaired electrons, each of which carries 1/2 spin and one Bohr magneton. This is consistent with

Lieb's theorem regarding the total spin $S = (n-1)/2$, which is dictated by the sublattice imbalance $N_A - N_B = n-1$ and thus $S=(N_A-N_B)/2$.

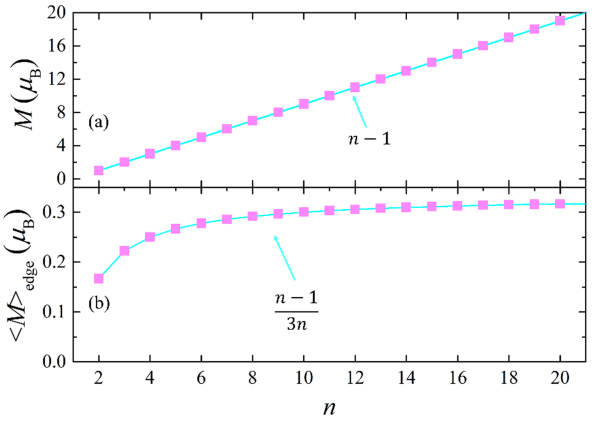

Fig. 4 (a) The linear scaling of total magnetic momentsM versus triangular size n of GNFs. Results calculated using three different energy functionals show no differences. (b) The average magnetic moment $\langle M\rangle_{edge}$ on the outermost edge atoms scales as $(n-1)/3n$ and converges to 1/3 μ_B for large n.

Now we address the size effects on the electronic and magnetic properties of triangular GNFs. Fig. 4 (a) shows the calculated net magnetic moments of n-GNFs as a function of size n. The distinctive topology of our quantum dots, coupled with the half-filled nature of graphene lattice, results in the presence of $(n-1)$ unpaired electrons. Our results confirms a linear scaling of the magnetic moment with the system size n as predicted by Lieb[32] based on a bipartite half-filled Hubbard model with repulsive interactions. We mentioned that we have carried out calculations using three different functionals, namely, the PBE, PBEsol, and LDA functionals, the results are practically identical. Thus, we only show the results calculated using the PBE functional. The net magnetic moment is found to be proportional to the edge size, i. e., $M = (n-1)\ \mu_B$, with n being the number of atoms on the A sublattice on one of the edges. Fig. 4 (b) shows the averaged local magnetic moment $\langle M\rangle_{edge} = (n-1)/3n$ on the outermost edge atoms as a function of n. The result converges to 1/3 μ_B in the large n limit.

The quantum confinement effects also have an important influence on the electronic properties, in particular, the energy gaps of these systems as shown in Fig. 5. We show the spin-flipping gaps calculated using three different functionals. In general, the PBE functional gives slightly larger gaps. The DFT-PBE (spin-flipped) gap varies from 0.24 to 0.69 eV for n-GNFs with n ranging from 2 to 20, decreasing monotonically (but moderately) for n greater than 3. Interestingly, the spin-preserving gap shows a much greater size dependence, decreasing from 2.70 eV for 2-GNF to 0.72 eV for 20-GNF. Although DFT calculations cannot give accurate predictions of the energy gap, our results still suggest that these triangular quantum dots may be used as building blocks for magnetic semiconductor and optoelectronic devices with size-tunable gaps[27,28,31].

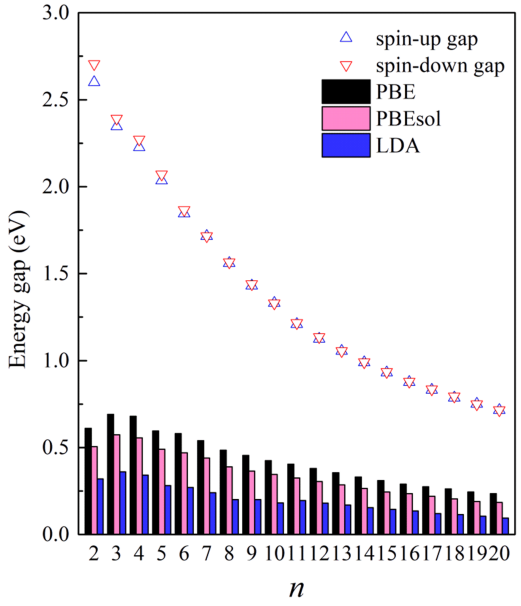

Fig. 5 Spin-preserving (open triangles) and spin-flipping (bars) energy gaps as a function of n. Only the PBE results are shown for the spin-preserving gaps.

4 Conclusion

In conclusion, we have investigated the electronic and magnetic properties of *triangular* shaped graphene nanoflakes using spin-polarized

DFT calculations. Our first-principles calculations demonstrate that the electronic and magnetic properties of *triangulene* are intimately related to their sizes. The minimization of the Coulomb energy leads to the localization of these unpaired electron on one the graphene sublattices, giving rise to a magnetic ground state. The net magnetic moment is found to be proportional to the edge size, i. e. , $M = (n-1)\mu_B$, with n being the number of atoms on the A sublattice on one of the edges. Interestingly, the average magnetic moment on the outermost edge atoms converges to a constant value $(n-1)/3n$ as the size of the quantum dot increases. The degree of degeneracy of the spin-polarized near-edge states is also equal to $n-1$. We show that the energy gaps, both the spin-preserving and spin-flipping ones, decrease as the size of GNFs increases as a result of diminishing quantum confinement effects. We believe that these systems provide a unique opportunity for designing quantum structures with a high degree of degeneracy, analogously to the two-dimensional electron gas in a strong magnetic field. The electronic and magnetic properties of GNFs thus open new avenues for utilizing triangular graphene in nanoscale magnetic semiconductor devices.

参 考 文 献

[1] T. Makarova and F. Palacio, *Carbon based magnetism: an overview of the magnetism of metal free carbon-based compounds and materials* (Elsevier, 2006).

[2] P. Dev, Y. Xue, and P. Zhang, *Phys. Rev. Lett.* **100**, (2008), 117204.

[3] K. S. Novoselov, A. K. Geim, S. V. Morozov, D. Jiang, Y. Zhang, S. V. Dubonos, I. V. Grigorieva, and A. A. Firsov, *Science* **306**, (2004), 666.

[4] K. S. Novoselov, A. K. Geim, S. V. Morozov, D. Jiang, M. I. Katsnelson, I. V. Grigorieva, S. V. Dubonos, and A. A. Firsov, *Nature* **438**, (2005), 197.

[5] B. Uchoa and A. H. Castro Neto, *Phys. Rev. Lett.* **98**, (2007), 146801.

[6] H. B. Heersche, P. Jarillo-Herrero, J. B. Oostinga, L. M. Vandersypen, and A. F. Morpurgo, *Nature* **446**, (2007), 56.

[7] A. H. Castro Neto, F. Guinea, N. M. R. Peres, K. S. Novoselov, and A. K. Geim, *Rev Mod Phys* **81**, (2009), 109.

[8] Y. Shibayama, H. Sato, T. Enoki, and M. Endo, *Phys. Rev. Lett.* **84**, (2000), 1744.

[9] O. V. Yazyev and M. I. Katsnelson, *Phys. Rev. Lett.* **100**, (2008), 047209.

[10] G. Z. Magda, X. Jin, I. Hagymási, P. Vancsó, Z. Osváth, P. Nemes-Incze, C. Hwang, L. P. Biró, and L. Tapasztó, *Nature* **514**, (2014), 608.

[11] E. J. Kan, Z. Li, J. Yang, and J. G. Hou, *J. Am. Chem. Soc.* **130**, (2008), 4224.

[12] P. Ruffieux, S. Wang, B. Yang, C. Sánchez-Sánchez, J. Liu, T. Dienel, L. Talirz, P. Shinde, C. A. Pignedoli, D. Passerone, T. Dumslaff, X. Feng, K. Müllen, and R. Fasel, *Nature* **531**, (2016), 489.

[13] Y. Lin and J. W. Connell, *Nanoscale* **4**, (2012), 6908.

[14] H. Feldner, Z. Y. Meng, A. Honecker, D. Cabra, S. Wessel, and F. F. Assaad, *Phys. Rev. B* **81**, (2010), 115416.

[15] Y. Ge, J. Ji, Z. Shen, Q. Zhang, A. Jian, Q. Duan, C. Wang, J. Jiang, W. Zhang, and S. Sang, *Carbon* **127**, (2018), 432.

[16] I. Hagymási and Ö. Legeza, *Phys. Rev. B* **97**, (2018), 035142.

[17] W. L. Wang, S. Meng, and E. Kaxiras, *Nano. Lett.* **8**, (2008), 241.

[18] H. Jin, J. Li, T. Wang, and Y. Yu, *Carbon* **137**, (2018), 1.

[19] G. Jo, M. Choe, S. Lee, W. Park, Y. H. Kahng, and T. Lee, *Nanotechnology* **23**, (2012), 112001.

[20] A. Reina, S. Thiele, X. Jia, S. Bhaviripudi, M. S. Dresselhaus, J. A. Schaefer, and J. Kong, *Nano Research* **2**, (2010), 509.

[21] C. Soldano, A. Mahmood, and E. Dujardin, *Carbon* **48**, (2010), 2127.

[22] J. Guttinger, T. Frey, C. Stampfer, T. Ihn, and K. Ensslin, *Phys. Rev. Lett.* **105**, (2010), 116801.

[23] P. G. Silvestrov and K. B. Efetov, *Phys. Rev. Lett.* **98**, (2007), 016802.

[24] B. Trauzettel, D. V. Bulaev, D. Loss, and G. Burkard, *Nat. Phys.* **3**, (2007), 192.

[25] E. Clar and D. G. Stewart, *J. Am. Chem. Soc.* **75**, (1953), 2667.

[26] I. Hagymási, P. Vancsó, A. Pálinkás, and Z. Osváth, *Phys. Rev. B* **95**, (2017), 075123.

[27] S. Mishra, D. Beyer, K. Eimre, J. Liu, R. Berger, O. Groning, C. A. Pignedoli, K. Mullen, R. Fasel, X. Feng, and P. Ruffieux, *J. Am. Chem. Soc.* **141**, (2019), 10621.

[28] J. Su, M. Telychko, P. Hu, G. Macam, P. Mutombo, H. Zhang, Y. Bao, F. Cheng, Z. Q. Huang, Z. Qiu, S. J. R. Tan, H. Lin, P. Jelinek, F. C. Chuang, J. Wu, and J. Lu, *Sci. Adv.* **5**, (2019), eaav7717.

[29] J. Li, S. Sanz, J. Castro-Esteban, M. Vilas-Varela, N. Friedrich, T. Frederiksen, D. Pena, and J. I. Pascual, *Phys. Rev. Lett.* **124**, (2020), 177201.

[30] J. Fernandez-Rossier and J. J. Palacios, *Phys. Rev. Lett.* **99**, (2007), 177204.

[31] Y. Morita, S. Suzuki, K. Sato, and T. Takui, *Nat. Chem.* **3**, (2011), 197.

[32] E. H. Lieb, *Phys. Rev. Lett.* **62**, (1989), 1201.

[33] P. E. Blöchl, *Phys. Rev. B* **50**, (1994), 17953.

[34] G. Kresse and D. Joubert, *Phys. Rev. B* **59**, (1999), 1758.

[35] G. Kresse and J. Furthmüller, *Phys. Rev. B* **54**, (1996), 11169.

[36] G. Kresse and J. Furthmüller, *Computational Materials Science* **6**, (1996), 15.

[37] W. Kohn and L. J. Sham, *Phys Rev* **140**, (1965), A1133.

[38] J. P. Perdew, K. Burke, and M. Ernzerhof, *Phys. Rev. Lett.* **77**, (1996), 3865.

[39] A. D. Becke, *Phys Rev A* **38**, (1988), 3098.

[40] J. P. Perdew, J. A. Chevary, S. H. Vosko, K. A. Jackson, M. R. Pederson, D. J. Singh, and C. Fiolhais, *Phys. Rev. B* **46**, (1992), 6671.

[41] J. P. Perdew, A. Ruzsinszky, G. I. Csonka, O. A. Vydrov, G. E. Scuseria, L. A. Constantin, X. Zhou, and K. Burke, *Phys. Rev. Lett.* **100**, (2008), 136406.

[42] K. Momma and F. Izumi, *J. Appl. Crystallogr* **44**, (2011), 1272.

[43] Y. Zheng, C. Li, C. Xu, D. Beyer, X. Yue, Y. Zhao, G. Wang, D. Guan, Y. Li, H. Zheng, C. Liu, J. Liu, X. Wang, W. Luo, X. Feng, S. Wang, and J. Jia, *Nat Com* **11**, (2020), 6076.

[44] H. Şahin, R. T. Senger, and S. Ciraci, *J Appl Phys* **108**, (2010), 074301.

[45] P. Potasz, A. D. Güçlü, and P. Hawrylak, *Phys. Rev. B* **81**, (2010), 033403.

[46] P. Potasz, A. D. Güçlü, A. Wójs, and P. Hawrylak, *Phys. Rev. B* **85**, (2012), 075431.